Journal of Power Sources 233 (2013) 394–400

Contents lists available at SciVerse ScienceDirect

Journal of Power Sources

journal homepage: www.elsevier.com/locate/jpowsour

Effect of TiC addition and high-temperature annealing on the microstructure and electrical conductivity of shrouded-plasma-sprayed FeAl/TiC composites for SOFC support

Li-Hui Tian, Cheng-Xin Li*, Guan-Jun Yang, Chang-Jiu Li

State Key Laboratory for Mechanical Behavior of Materials, School of Materials Science and Engineering, Xi'an Jiaotong University, 28 Xian-Ning West-Road, Xi'an, Shaanxi 710049, China

HIGHLIGHTS

- Dense FeAl and FeAl/TiC coatings were deposited by shrouded plasma spraying.
- High-temperature annealing leads to the change in the shape of interlamellar gaps.
- The coating electrical conductivity is increased as the annealing time is increased.
- The RT electrical conductivity is about 90% of the bulks when annealed for over 10 h.
- The RT electrical conductivity was increased by 49% when 45 vol.% TiC was added.

ARTICLE INFO

Article history:
Received 7 October 2012
Received in revised form
4 January 2013
Accepted 5 January 2013
Available online 24 January 2013

Keywords:
Solid oxide fuel cells
Support
Iron aluminide intermetallics
Shrouded plasma spraying
Annealing
Electrical conductivity

ABSTRACT

FeAl and FeAl/TiC coatings are deposited by shrouded plasma spraying. The microstructure of the as-sprayed and annealed coatings is characterized by scanning electron microscopy. The electrical conductivity of the coatings along the direction parallel to the coating surface is measured. Results show that the as-sprayed coatings exhibit lower electrical conductivity than that of the corresponding bulks, which is due to their inherent lamellar microstructure. The thin interlamellar gaps become more spherical pores and the metallurgical bonding regions are increased by high-temperature annealing due to solid-state diffusion between flattened splats. The electrical conductivity of the coatings increases with the increase of the annealing time. The room temperature electrical conductivity of the coatings annealed at 1100 °C for over 10 h reaches to about 90% of that of the corresponding bulks. Besides, it is found that the electrical conductivity of the FeAl/TiC coatings increases with the increase of the TiC content. When 45 vol.% TiC is added into the FeAl matrix, the electrical conductivity of the FeAl/TiC coating annealed at 1100 °C reaches 5.35×10^3 S cm^{-1} at 1000 °C, which is much higher than that of the commonly used Ni/YSZ support material in solid oxide fuel cells.

1. Introduction

Solid oxide fuel cells (SOFCs), which can directly convert chemical energy of fuel gases into electrical power, are promising candidates for future power generation systems due to their advantages, such as high power conversion efficiency, environmentally benign, cogeneration capability, and flexibility in fuel use [1,2]. A typical SOFC system is usually composed of three basic functional layers, i.e., an electrolyte layer, an anode layer and a cathode layer. A support layer is always necessary to mechanically stabilize the functional layers when being prepared and operating. As the support layer in the SOFC system, some characteristics, such as a certain high-temperature strength, appropriate thermal expansion matching with the other components (especially the electrolyte), high electrical conductivity, and low material cost are necessary. It is reported that the functional layers have been widely used as the supports in SOFC systems. In an electrolyte (yttria-stabilized zirconia, YSZ)-supported SOFC, a thick (about 1 mm) YSZ layer is required due to its poor mechanical strength, which may result in cell breakage and stack failure when being prepared and operating [3]. Moreover, the high thickness of the electrolyte layer can lead to a reduction of cell performance due to its low conductivity [4]. For the cathode support, besides the poor mechanical strength, the need of lots of cathode materials, such as strontium

* Corresponding author. Tel.: +86 29 82665299; fax: +86 29 83237910.
E-mail addresses: licx@mail.xjtu.edu.cn (C.-X. Li), licj@mail.xjtu.edu.cn (C.-J. Li).

0378-7753/$ – see front matter © 2013 Elsevier B.V. All rights reserved.
http://dx.doi.org/10.1016/j.jpowsour.2013.01.074

doped lanthanium manganate, can also significantly increase the cost of the cells due to their high prices. The anode (Ni–YSZ) support design was widely adopted because of its lower cost than that of electrolytic and cathodic materials. However, it has been found that anode support also has a low mechanical strength at high temperatures due to the poor strength of nickel above 600 °C.

Recently, iron aluminides are promising high-temperature structural materials used in hostile environments owing to their attractive mechanical, physical and chemical properties such as high strength [5–8], high melting point [9], low density [10–12], high oxidation resistance [12–14], high sulfidation resistance [7,15–17] and low material cost [11,18]. In the previous study [19], FeAl and FeAl/TiC coatings were deposited by shrouded plasma spraying. The effect of the TiC content on the thermal expansion behavior of FeAl/TiC coatings was investigated. The results showed that the mean coefficients of thermal expansion (CTE) of FeAl/TiC coatings can be properly controlled by adjusting the volume fraction of TiC besides the strengthening of the FeAl matrix [10], and when 45 vol.% TiC was added into the FeAl matrix, a mean CTE of $11.4 \times 10^{-6}\ °C^{-1}$ was obtained, which is nearly the same as that of the components in SOFC, especially the electrolyte. Therefore, FeAl/TiC composite maybe a potential support material in SOFCs owing to the above advantages. In a FeAl/TiC composite-supported tubular SOFC design, the FeAl/TiC layer plays dual roles of a support tube and an electrode current collector, where high electrical conductivity along the direction parallel to the coating surface is necessary to reduce the internal resistance and increase the output performance of the cell.

Therefore, in this study, as a further investigation on this potential support material in SOFCs, the effect of the TiC addition and high-temperature annealing on the coating microstructure and electrical conductivity were investigated.

2. Experimental

2.1. Feedstock powder and coating preparation

Fe-35 at.% Al (Fe–Al), Fe-35 at.% Al/35 vol.% TiC (Fe–Al/35TiC) and Fe-35 at.% Al/45 vol.% TiC (Fe–Al/45TiC) powders prepared by ball milling were used as the feedstocks. A high-energy plasma spray system (GP-80, 80 kW class, JIUJIANG, China) attached with a shrouding cylindrical nozzle shown schematically in Fig. 1 was used to deposit the coatings. To prevent the feedstocks from oxidation, nitrogen was used as a protective gas during spraying. FeAl, FeAl/35TiC and FeAl/45TiC coatings were deposited on a 1Cr18Ni9Ti stainless steel substrate at the same stand-off distance of 150 mm and different plasma arc powers of 20, 20 and 30 kW, respectively. Further details about spray processing conditions can be found in the previous paper [19].

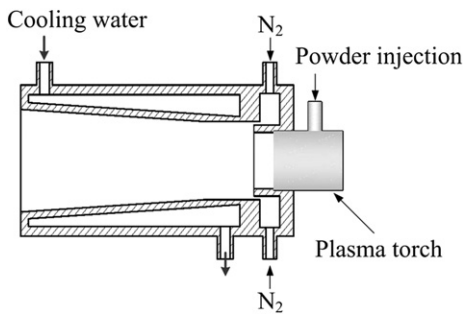

Fig. 1. Sketch of the shrouding nozzle.

2.2. Microstructure characterization

Cross sectional microstructure characterization of the coatings was carried out using scanning electron microscopy (SEM, VEGA II XMU, TESCAN, Czech Republic) coupled with energy dispersive X-ray analysis (EDXA, 7718, Oxford Instruments, England). The porosity of the coatings was determined by image analyzing. For each coating, ten cross-sectional images at a magnification of 2000 were analyzed to provide an average value.

2.3. Electrical conductivity measurement

The electrical resistances of the coatings along the direction parallel to the coating surfaces were measured by a Kelvin bridge (QJ57). The coatings were deposited thick enough during spraying to be easily detached from the substrate and obtain free-standing deposits. The testing specimens with the dimensions of $10 \times 35 \times 2$ mm (width, length and thickness) were cut out from the free-standing deposits by electrical discharge machining and then annealed at 1100 °C for 5, 10, 15 and 20 h in an argon atmosphere. Before the measurement, the surfaces of the specimens were polished using emery paper. Four platinum lead wires were fixed on the specimen using platinum paste, which is shown in Fig. 2. To ensure a good contact between the lead wires and the specimen, the pasted specimen was dried at 100 °C for 30 min and sintered at 900 °C for 30 min in an argon atmosphere. To prevent the specimens from oxidation during testing, the electrical resistance was measured in an argon atmosphere. The testing temperature range was from room temperature to 1000 °C and the heating rate was 5 °C min^{-1}. The electrical conductivity of the specimens was calculated from $\sigma = L/RS$, where σ was the electrical conductivity, L was the effective length between P_{x1} and P_{x2} (Fig. 2), R was the electrical resistance, and S was the cross-sectional area in the direction perpendicular to the current flow. Three measurements were performed for each coating to provide an average value.

3. Results and discussion

3.1. Microstructure of the as-sprayed FeAl and FeAl/TiC coatings

A general microstructural feature of the as-sprayed coatings was reported in the previous paper [19]. As a further investigation,

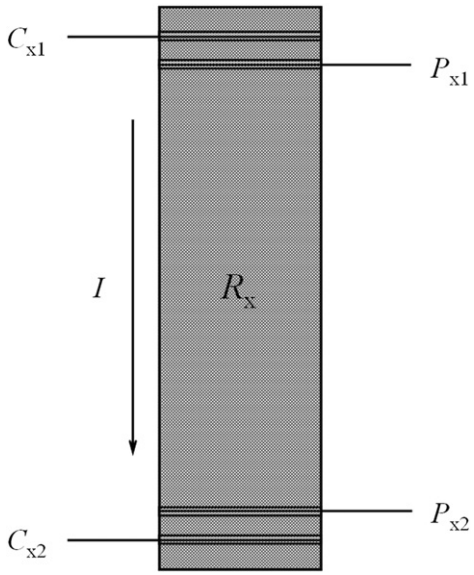

Fig. 2. Sketch of the specimen for measuring the electrical resistance.

a detailed examination of their microstructure was carried out in this study. Figs. 3–5 show the typical cross-sectional microstructure of the as-sprayed FeAl, FeAl/35TiC and FeAl/45TiC coatings, respectively. It can be seen that the coatings exhibited a typical lamellar microstructure. Most of the spray particles in the coatings were exhibited as well flattened splats. This fact suggests that the feedstock powder particles have been heated to sufficiently molten droplets once they are fed into the plasma jet.

Generally, three types of voids, i.e., three-dimensional-type (3D-type), two-dimensional-type (2D-type) and microcrack-type voids exist in the thermal spray coatings [20]. The voids present in the as-sprayed FeAl and FeAl/TiC coatings are shown in Figs. 3–5. The 3D-type voids, i.e., the coarse pores in a size range from sub-micrometers to several micrometers, are due to the incomplete wetting and insufficient filling of the fully molten droplets to previously formed rough deposit surfaces [21]. The 2D-type voids, i.e., the interlamellar gaps with the dimension of sub-micrometers at the direction perpendicular to splat plane, are very thin regions of no contact at the interfaces between the fully molten splats, which may arise from the gas entrapped beneath the spreading droplets [22] or insufficient wetting of spreading melt to the underlying solid surface due to low interface contact temperature [23]. The microcracks perpendicular to splat plane often occur in the flattened splats deposited with brittle materials, such as ceramics due to the quenching stress [24,25]. For the FeAl and FeAl/TiC coatings deposited with metallic materials, the cracks can be neglected. However, the splat peripheries present in the coatings can be regarded as such cracks [20].

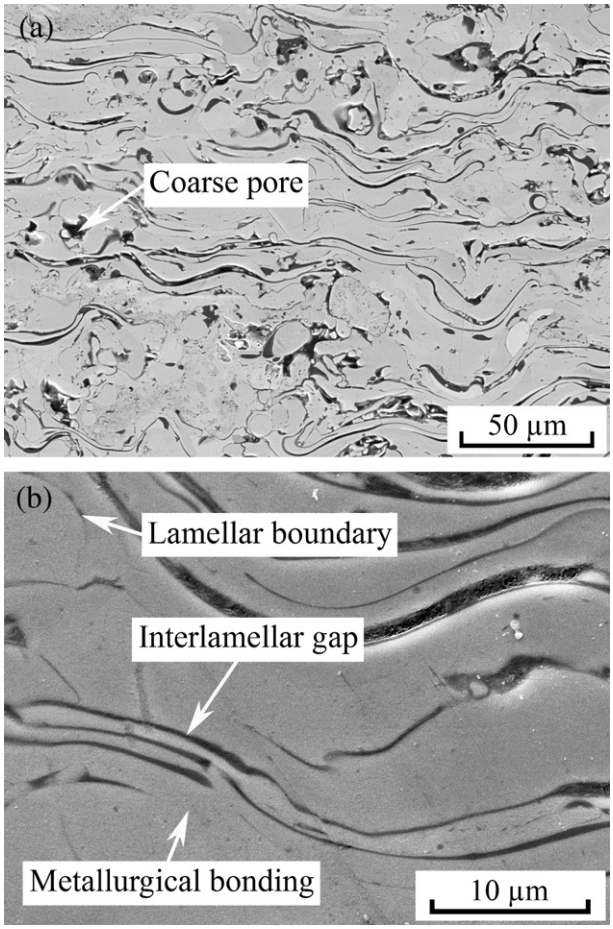

Fig. 3. Images of the as-sprayed FeAl coating at a lower magnification (a) and a higher magnification (b).

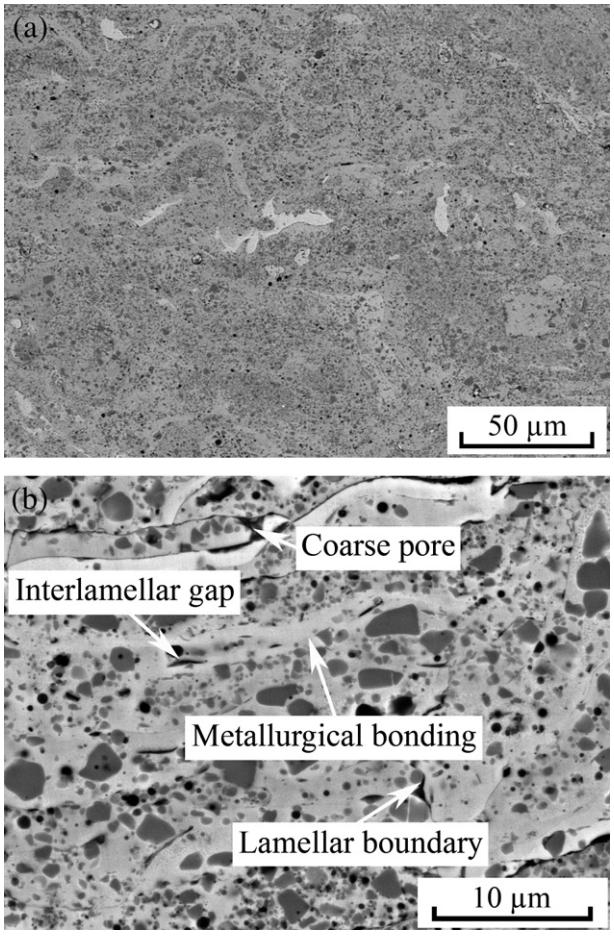

Fig. 4. Images of the as-sprayed FeAl/35TiC coating at a lower magnification (a) and a higher magnification (b).

Besides interlamellar gaps, it is clearly observed that metallurgical bonding regions were formed at some local interfaces between the well flattened splats (as marked by arrows in Figs. 3b, 4b and 5b). The formation of the metallurgical bonding regions can be associated with the possible remelting of the previously deposited splats upon impact of fully molten high-temperature droplets. The feedstock powder particles are heated to fully molten droplets with a temperature higher than their melting points once they are fed into the high-temperature plasma jet. With the mechanically alloyed Fe–Al powder, it was recognized that the reaction between iron and aluminum elements occurs to form FeAl intermetallics [19]. Since the reaction is exothermic [26–28], the temperature of molten particles will be further raised by the additional heat. Thus, when the high-temperature droplets impact on the surfaces of the previously deposited splats, metallurgical bondings are formed at some local interfaces between the impacting droplets and the previously deposited splats due to its remelting [29].

3.2. Effect of annealing on the microstructure of the FeAl and FeAl/TiC coatings

Fig. 6 shows the microstructure of the FeAl coatings annealed at 1100 °C for different durations. It can be found that the microstructure of the coating annealed for 5 h is nearly the same as that of the as-sprayed one. However, when the annealing time was increased to 10 h, the coating microstructure became significantly

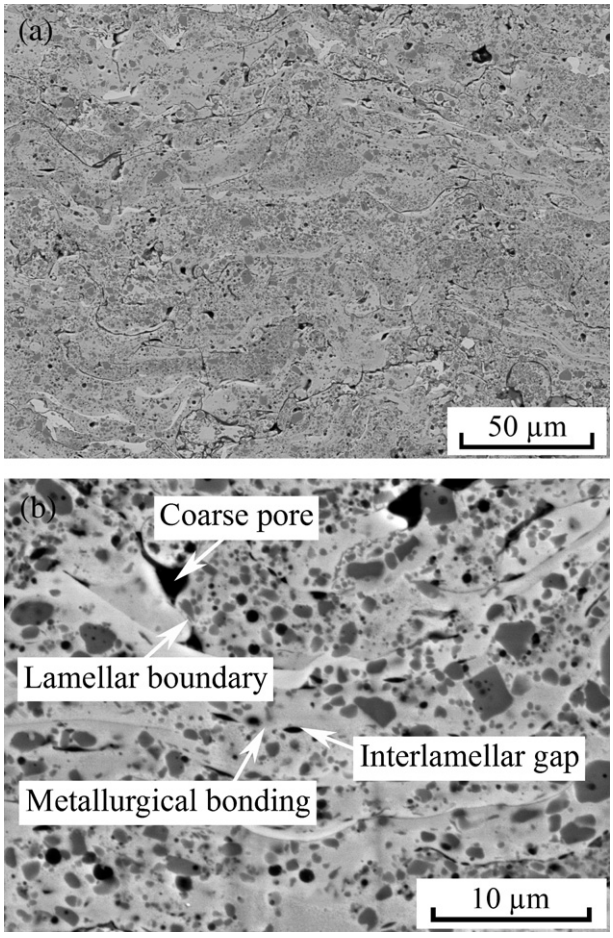

Fig. 5. Images of the as-sprayed FeAl/45TiC coating at a lower magnification (a) and a higher magnification (b).

different from that of the one annealed for 5 h. Most of the 2D-type voids, i.e., the interlamellar gaps disappeared and spherical pores appeared, which suggests that solid-state diffusion occurred between flattened splats during high-temperature annealing. With the increase of annealing time, i.e., to 15 and 20 h, the interlamellar gaps apparently became healed gradually. As the annealing time was increased to 20 h, the interlamellar gaps disappeared completely, and spherical pores were present in the coating as the main voids. Moreover, the splat peripheries were also decreased with annealing time and finally disappeared. The change of the shape of the interlamellar gaps from thin gaps to spherical pores was also reported when a plasma-sprayed CaO-stabilized ZrO_2 coating was subjected to a high-temperature annealing [30].

For the FeAl/TiC coatings, similar evolution of the coating microstructure with the annealing time was observed. The microstructures of the FeAl/35TiC and FeAl/45TiC coatings annealed at 1100 °C for 20 h are shown in Fig. 7a and b, respectively. It can be seen that after annealed for 20 h, the interlamellar gaps and the splat peripheries in the coatings disappeared, and spherical pores were present as the main voids.

The porosity of the coatings annealed at 1100 °C for different durations was estimated by image analyzing. From the results listed in Table 1, it can be seen that the porosity changed little with the annealing time. However, it was larger than that of the as-sprayed coatings reported previously [19], which is attributed to the coalescence of interlamellar gaps.

3.3. Relationship between microstructure and electrical conductivity of the as-sprayed and annealed FeAl and FeAl/TiC coatings

Fig. 8 shows the electrical conductivity measured as a function of testing temperature for the annealed FeAl and FeAl/35TiC coatings. The electrical conductivity of three coatings annealed for 20 h is shown in Fig. 9. As the annealing time was increased to 10 h, the electrical conductivity was increased significantly (Fig. 8). With

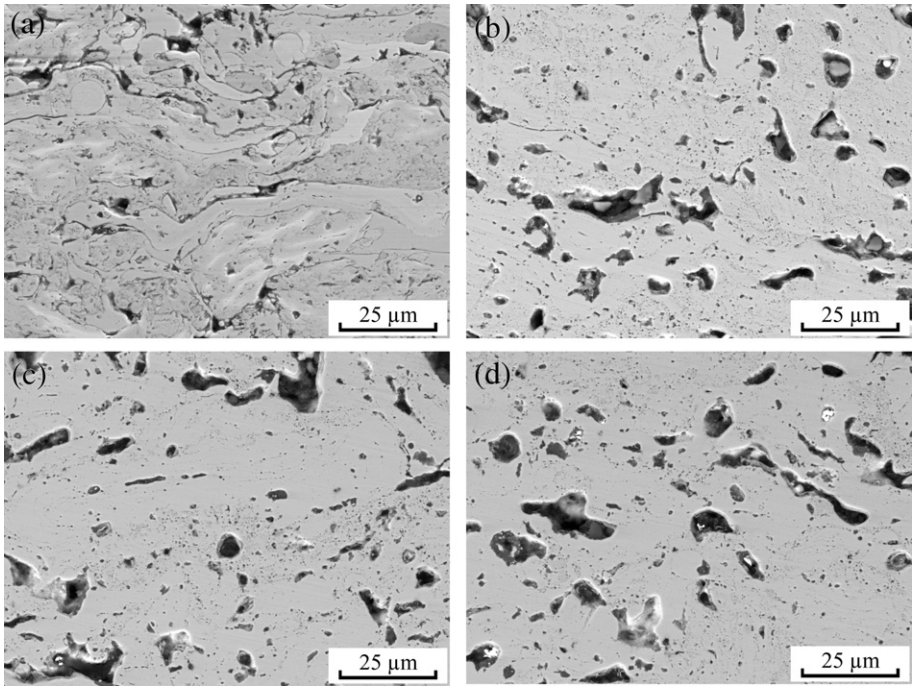

Fig. 6. Images of the FeAl coating annealed at 1100 °C for different durations. (a) 5 h. (b) 10 h. (c) 15 h. (d) 20 h.

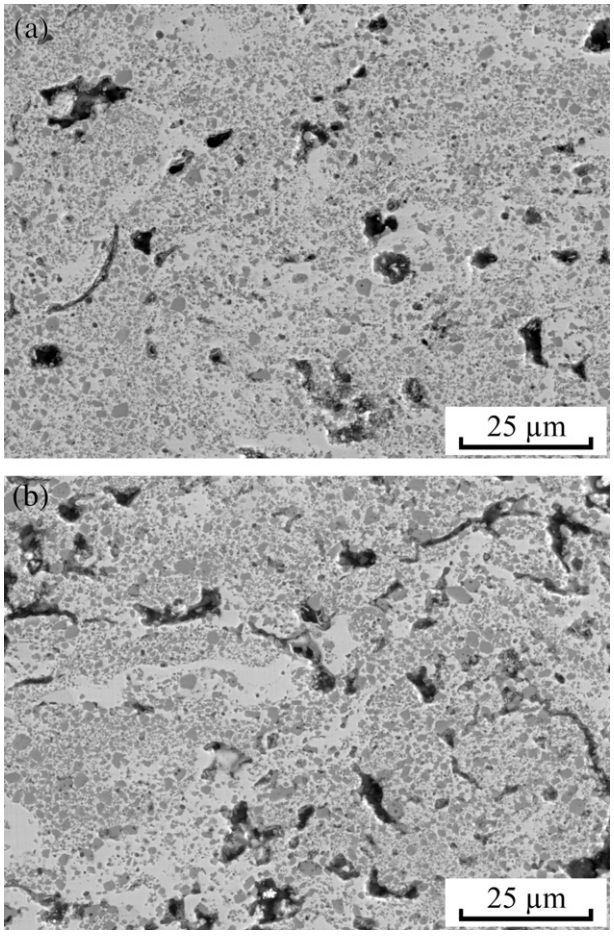

Fig. 7. Images of the FeAl/TiC composite coatings annealed at 1100 °C for 20 h. (a) FeAl/35TiC coating. (b) FeAl/45TiC coating.

a further increase in annealing time, the increase of the electrical conductivity became not significant. Moreover, compared to the electrical conductivity of the FeAl/TiC coatings annealed for 20 h with that of the FeAl coating annealed on the same condition, it was found that as the TiC content is increased, the electrical conductivity of the FeAl/TiC coatings is increased (Fig. 9).

In order to investigate the relationship between coating microstructure and electrical conductivity, the room temperature electrical conductivity of FeAl/TiC bulks was estimated theoretically based on the following formula [31],

$$\sigma_{\mathrm{FeAl/TiC}} = \sigma_{\mathrm{FeAl}} \frac{L\sigma_{\mathrm{TiC}} + (1-L)\sigma_{\mathrm{FeAl}} + f(1-L)(\sigma_{\mathrm{TiC}} - \sigma_{\mathrm{FeAl}})}{L\sigma_{\mathrm{TiC}} + (1-L)\sigma_{\mathrm{FeAl}} - fL(\sigma_{\mathrm{TiC}} - \sigma_{\mathrm{FeAl}})} \quad (1)$$

where the subscripts "FeAl/TiC", "FeAl" and "TiC" correspond to the electrical conductivity of bulk FeAl/TiC, bulk FeAl and bulk TiC, respectively. σ, L and f are the electrical conductivity, the depolarization factor of ellipsoids in the direction of current flow (1/3 for spherical TiC particles) and the volume fraction of TiC particles, respectively. For the estimation, the room temperature electrical conductivities of bulk FeAl (6.37×10^3 S cm^{-1}) and bulk TiC (14.71×10^3 S cm^{-1}) reported in the publications [32,33] were used. Table 2 shows the room temperature electrical conductivity of the as-sprayed and annealed coatings and the corresponding bulks.

Table 1
Porosity of the coatings annealed at 1100 °C for different durations.

Annealing time (h)	Porosity (%)		
	FeAl	FeAl/35TiC	FeAl/45TiC
5	4.8	5.3	–
10	5.0	5.7	–
15	4.3	5.4	–
20	4.4	5.3	6.3

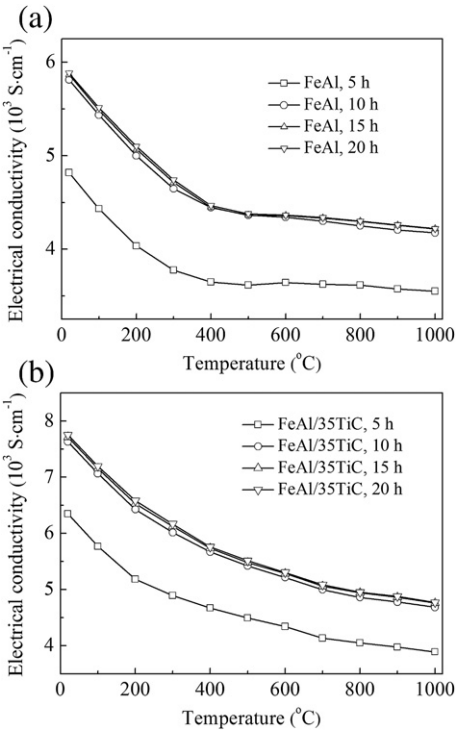

Fig. 8. Electrical conductivity of the annealed FeAl (a) and FeAl/35TiC coatings (b) as a function of temperature.

It can be seen from Table 2 that bulk FeAl has an electrical conductivity higher than that of the as-sprayed FeAl coating, and the electrical conductivity of the bulk FeAl/35TiC and FeAl/45TiC composites estimated based on Eq. (1) is higher than that of the corresponding as-sprayed coatings. The electrical conductivity of the as-sprayed coatings is about three-fourths of that of the corresponding bulks, which is attributed to their inherent lamellar microstructure.

As discussed in Section 3.1, coarse pores, interlamellar gaps and splat peripheries were present in the as-sprayed coatings. The theoretical relationship between electrical conductivity and

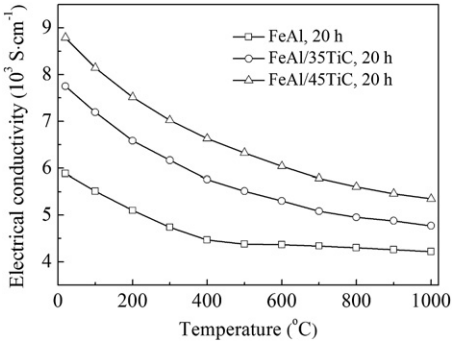

Fig. 9. Electrical conductivity of the FeAl and FeAl/TiC coatings annealed for 20 h.

Table 2
Room temperature electrical conductivity of the FeAl and FeAl/TiC coatings and the corresponding bulks ($\times 10^3$ S cm^{-1}).

	FeAl	FeAl/35TiC	FeAl/45TiC
As-sprayed	4.76 ± 0.01	6.27 ± 0.02	6.91 ± 0.03
Annealed, 1100 °C, 5 h	4.82 ± 0.01	6.35 ± 0.02	–
Annealed, 1100 °C, 10 h	5.81 ± 0.02	7.63 ± 0.03	–
Annealed, 1100 °C, 15 h	5.87 ± 0.03	7.71 ± 0.03	–
Annealed, 1100 °C, 20 h	5.88 ± 0.03	7.75 ± 0.04	8.79 ± 0.05
Bulk material	6.37	8.64	9.40

porosity in porous materials with dispersed spherical pores can be expressed as Ref. [31]:

$$\sigma = \sigma_{\text{Bulk}} \frac{1 - L - f(1 - L)}{1 - L + fL} \quad (2)$$

where σ and σ_{Bulk} are the electrical conductivity of porous material and bulk material, respectively. L and f are the depolarization factor of ellipsoids in the direction of current flow (1/3 for spherical pores) and the porosity of porous material, respectively. As reported in Ref. [19], the total porosities of the as-sprayed FeAl, FeAl/35TiC and FeAl/45TiC coatings were about 1.9, 1.6 and 1.9%, respectively. This fact indicates that the influence of the limited coarse pores on the electrical conductivity can be neglected based on Eq. (2).

Although the microcracks in the flattened splats of the coatings can be neglected, the splat peripheries, which can be regarded as such cracks, can not be neglected when considering the electrical conductivity along the direction parallel to the coating surfaces. For the coating without the splat peripheries, electrons can transfer directly along the direction parallel to the coating surfaces through splat layer from point "A" to point "B" as marked by dashed line schematically shown in Fig. 10. However, in the case of the coating with the splat peripheries, electrons will transfer from "A" through "C" and finally to "B". An extra contact resistance $r_A + r_B = 2r_c = 1/\sigma a$ is expected [34], where r_c is the contact resistance for one contact area, σ is the electrical conductivity of bulk material, and a is the radius of the contact area. Therefore, the lower electrical conductivity of the as-sprayed coatings is attributed to the presence of the splat peripheries.

In addition, for a lamellar interface in which there are n such contacts, the total contact resistance can be expressed as $R_c = r_c/n = 1/2n\sigma a$. Therefore, the metallurgical bonding regions at some local interfaces have a positive influence, while the interlamellar gaps have a negative influence on the increase of the electrical conductivity.

It can be seen from Fig. 8 and Table 2 that as the annealing time is increased, the electrical conductivity of the coatings is increased. As discussed in Section 3.2, the microstructure of the coatings annealed for 5 h was nearly the same as that of the as-sprayed ones. Being similar to the as-sprayed coatings, the interlamellar gaps and the splat peripheries which have a significant influence on the electrical conductivity are still present in the coatings. Therefore, the electrical conductivity of the coatings annealed for 5 h was nearly the same as that of the as-sprayed ones, i.e., about three-fourths of that of the corresponding bulks. As the annealing time was increased to 10 h, the interlamellar gaps, especially the splat peripheries apparently become healed, and the electrons can transfer directly along the direction parallel to the coating surfaces. Therefore, the electrical conductivity was increased significantly to about 90% of the corresponding bulk materials. With further increase of annealing time from 10 h to 20 h, the change of the electrical conductivity become less significant.

The room temperature electrical conductivity of the annealed coatings was theoretically estimated based on Eq. (2). For the estimation, the porosity of the coatings listed in Table 1 and the electrical conductivity of the bulks listed in Table 2 were used. The estimated results are shown in Fig. 11 in comparison with the data measured for the corresponding coatings.

It can be observed from Fig. 11 that the room temperature electrical conductivity estimated for the coatings annealed for 5 h is much higher than the data measured in the present study, and the estimated data for the coatings annealed for 10, 15, and 20 h are well consistent with the measured data. As discussed above, the coatings annealed for 5 h are not presented as simple porous materials due to the presence of the interlamellar gaps and splat peripheries, and Eq. (2) is not suitable for the estimation of their electrical conductivity. Accordingly, the electrical conductivity estimated was much higher than the data measured. However, with the increase of annealing time, i.e., to 10, 15 and 20 h, the interlamellar gaps and the splat peripheries apparently become healed gradually, and finally changed to spherical pores. In this case, Eq. (2) can be used to estimate the electrical conductivity of the porous coatings, and the estimated data were well consistent with those measured data.

As mentioned above, the electrical conductivity increases with the increase of the TiC content (Fig. 9). For the as-sprayed coatings and the coatings annealed for shorter time, for example, 5, 10 and 15 h, there are many factors influencing the electrical conductivity, such as coarse pores, interlamellar gaps and splat peripheries. However, for the coatings annealed for 20 h, the factors influencing the electrical conductivity are the TiC content and the porosity. Therefore, the electrical conductivity of the coatings annealed for 20 h is used to investigate the effect of TiC content on the electrical conductivity. Image analyzing was carried out to estimate the porosity of them, and similar porosities of 4.4, 5.3 and 6.3% were yielded for FeAl, FeAl/35TiC and FeAl/45TiC coatings, respectively (Table 1). Based on Eq. (2), the effect of the difference in porosity on the electrical conductivity can be neglected. Therefore, the only factor influencing the electrical conductivity is the TiC content. It can be seen from Table 2 that bulk FeAl has an electrical conductivity of about 6.37 $\times$ 10^3 S cm^{-1} [32], while that of bulk TiC is about 14.71 $\times$ 10^3 S cm^{-1} [33], which is higher than that of bulk FeAl. From

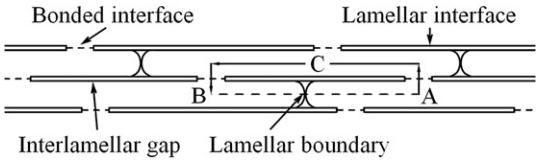

Fig. 10. Schematic view of the coating cross-sectional microstructure.

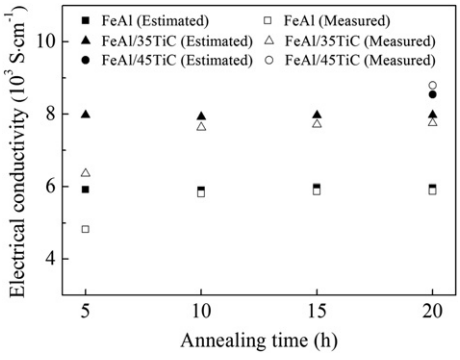

Fig. 11. Comparison of the measured and estimated room temperature electrical conductivity for the FeAl and FeAl/TiC coatings annealed for different durations.

the electrical conductivity of bulk FeAl/TiC composites estimated based on Eq. (1), it is obvious that the addition of the TiC ceramic phase can increase the room temperature electrical conductivities by 36 and 48% for FeAl/35TiC and FeAl/45TiC composites, respectively. Comparing the room temperature electrical conductivity of the FeAl/TiC composite coatings annealed for 20 h with that of the FeAl coating annealed on the same condition, it was found that the electrical conductivities of the FeAl/35TiC and FeAl/45TiC composite coatings were approximately 32 and 49% higher than that of the FeAl coating, which is consistent with the estimated results of the bulks.

At a testing temperature of 1000 °C, FeAl coating showed a lower electrical conductivity of 4.22×10^3 S cm^{-1}, while those of the FeAl/35TiC and FeAl/45TiC coatings were approximately 13 and 27% higher than that of the FeAl coating. Besides, it was found that the electrical conductivity of the FeAl/45TiC composite coating annealed for 20 h reached 5.35×10^3 S cm^{-1} at 1000 °C, which is much higher than that of the commonly used Ni/YSZ [35] cermet support material in SOFCs. Therefore, FeAl/45TiC composite material is a potential support material in SOFCs owing to its high strength [10], appropriate thermal expansion [19], and high electrical conductivity.

4. Conclusions

The as-sprayed FeAl and FeAl/TiC coatings showed lower electrical conductivity than that of the corresponding bulks. The thin interlamellar gaps became more spherical pores and the metallurgical bonding regions were increased during high-temperature annealing due to solid-state diffusion between flattened splats. As the annealing time was increased up to 10 h at 1100 °C, the electrical conductivity of the coatings was significantly increased. The room temperature electrical conductivity of the coatings annealed at 1100 °C for 10 h reached to about 90% of that of the corresponding bulks. With further increasing annealing time, the improvement of the electrical conductivity becomes less significant.

The electrical conductivity of the FeAl/TiC coatings increased with the increase of the TiC content. Comparing with the FeAl coating, the addition of the TiC ceramic phase increased the room temperature electrical conductivities by 32 and 49% for FeAl/35TiC and FeAl/45TiC composite coatings, respectively. The electrical conductivities of the FeAl/35TiC and FeAl/45TiC composite coatings were approximately 13 and 27% higher than that of the FeAl coating at 1000 °C. The electrical conductivity of the annealed FeAl/45TiC coating reached 5.35×10^3 S cm^{-1} at 1000 °C. Therefore, FeAl/45TiC composite material is a potential support material in SOFCs owing to its appropriate thermal expansion, high strength, and high electrical conductivity.

Acknowledgments

The present work is supported by the National Science Fund for Distinguished Young Scholars of China (No. 50725101).

References

[1] M.C. Williams, J.P. Strakey, S.C. Singhal, J. Power Sources 131 (2004) 79.
[2] A. Weber, E.I. Tiffée, J. Power Sources 127 (2004) 273.
[3] Z.W. Wang, J.O. Berghaus, S. Yick, C.D. Petit, W. Qu, R. Hui, R. Maric, D. Ghosh, J. Power Sources 176 (2008) 90.
[4] D. Rotureau, J.P. Viricelle, C. Pijolat, N. Caillol, M. Pijolat, J. Eur. Ceram. Soc. 25 (2005) 2633.
[5] M. Kupka, Intermetallics 14 (2006) 149.
[6] M. Kupka, J. Alloys Compd. 437 (2007) 373.
[7] S. Izadi, K. Janghorban, G.H. Akbari, M. Ghafari, E. Salahinejad, J. Alloys Compd. 493 (2010) 645.
[8] K. Yoshimi, S. Hanada, M.H. Yoo, Intermetallics 4 (1996) 159.
[9] N.S. Stoloff, C.T. Liu, S.C. Deevi, Intermetallics 8 (2000) 1313.
[10] M. Krasnowski, T. Kulik, J. Alloys Compd. 448 (2008) 227.
[11] G. Ji, T. Grosdidier, F. Bernard, S. Paris, E. Gaffet, S. Launois, J. Alloys Compd. 434–435 (2007) 358.
[12] N. Masahashi, S. Watanabe, S. Hanada, ISIJ Int. 41 (2001) 1010.
[13] S.E. Haghighi, K. Janghorban, S. Izadi, J. Alloys Compd. 503 (2010) 375.
[14] J.M. Guilemany, N. Cinca, S. Dosta, C.R.C. Lima, Intermetallics 15 (2007) 1384.
[15] P.C. Patnaik, W.W. Smeltzer, J. Electrochem. Soc. 132 (1985) 1226.
[16] P.F. Tortorelli, K. Natesan, Mater. Sci. Eng. A 258 (1998) 115.
[17] P.F. Tortorelli, J.H. DeVan, Mater. Sci. Eng. A 153 (1992) 573.
[18] N.S. Stoloff, Mater. Sci. Eng. A 258 (1998) 1.
[19] L.H. Tian, C.X. Li, C.J. Li, G.J. Yang, J. Therm. Spray Technol. 21 (2012) 689.
[20] C.J. Li, A. Ohmori, J. Therm. Spray Technol. 11 (2002) 365.
[21] C.J. Li, A. Ohmori, R. Mcpherson, J. Mater. Sci. 32 (1997) 997.
[22] R. Mcpherson, Thin Solid Films 83 (1981) 297.
[23] Y.Z. Xing, C.J. Li, C.X. Li, G.J. Yang, J. Power Sources 176 (2008) 31.
[24] C.J. Li, W.Z. Wang, Mater. Sci. Eng. A 386 (2004) 10.
[25] S. Kuroda, T.W. Clyne, Thin Solid Films 200 (1991) 49.
[26] H.W. Shi, D.B. Guo, Y.F. Ouyang, J. Alloys Compd. 455 (2008) 207.
[27] M. Krasnowski, A. Grabias, T. Kulik, J. Alloys Compd. 424 (2006) 119.
[28] F. Charlot, E. Gaffet, B. Zeghmati, F. Bernard, J.C. Niepce, Mater. Sci. Eng. A 262 (1999) 279.
[29] L. Li, X.Y. Wang, G. Wei, A. Vaidya, H. Zhang, S. Sampath, Thin Solid Films 468 (2004) 113.
[30] R. Brandt, High Temp. High Pressures 13 (1981) 79.
[31] A. Bjorneklett, L. Haukeland, J. Wigren, H. Kristiansen, J. Mater. Sci. 29 (1994) 4043.
[32] A.C. Lilly, S.C. Deevi, Z.P. Gibbs, Mater. Sci. Eng. A 258 (1998) 42.
[33] H.O. Pierson, Handbook of Refractory Carbides and Nitrides: Properties, Characteristics, Processing and Applications, first ed., Noyes Publications, New York, 1996.
[34] R. Mcpherson, Thin Solid Films 112 (1984) 89.
[35] D.W. Dees, T.D. Clarr, T.E. Easler, D.C. Fee, F.C. Mrazek, J. Electrochem. Soc. 134 (1987) 2141.